JACS
JOURNAL OF THE AMERICAN CHEMICAL SOCIETY

Article

pubs.acs.org/JACS

Impact of Regiochemistry and Isoelectronic Bridgehead Substitution on the Molecular Shape and Bulk Organization of Narrow Bandgap Chromophores

Gregory C. Welch,[†,§] Ronald C. Bakus, II,[†] Simon J. Teat,[‡] and Guillermo C. Bazan*[,†]

[†]Center for Polymers and Organic Solids, Departments of Chemistry & Biochemistry and Materials, University of California, Santa Barbara, California 93106, United States

[‡]Advanced Light Source, Lawrence Berkeley National Laboratory, 1 Cyclotron Road, Mail Stop 15-317, Berkeley, California 94720, United States

Supporting Information

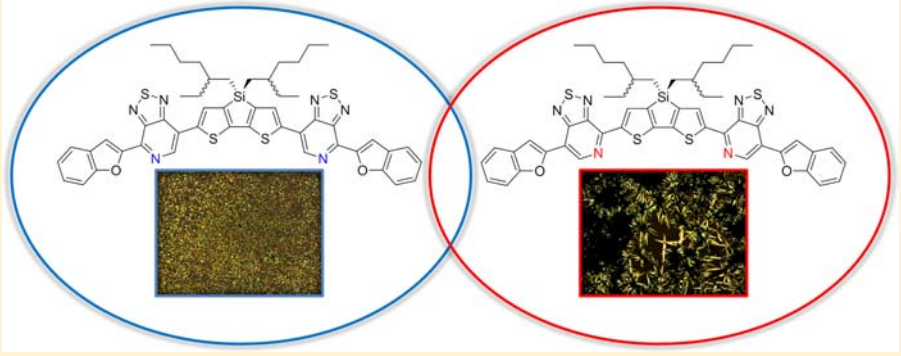

ABSTRACT: A comparison of two classes of small molecules relevant to the field of organic electronics is carried out at the molecular and supramolecular levels. First, two molecules that differ only in the position of a pyridyl N-atom within an acceptor fragment are compared and contrasted. X-ray investigation of single crystals reveals that positioning the pyridyl N-atoms *proximal* to the molecules center changes the molecular shape by bending the molecule into a banana shape. Second, we demonstrate that the banana shape of the molecule can be controlled by replacing a Si atom within the dithienosilole fragment with a C or Ge atom. Here, utilization of cyclopentadithiophene or dithienogermole as the internal electron-rich unit leads to a decrease or an increase in the bending of the conjugated backbone, respectively. Such molecular shape changes alter intermolecular packing and thus affect bulk properties, leading to large differences in the optical, thermal, and crystallization properties.

INTRODUCTION

Molecular self-assembly into functional nanostructures and extended networks is of importance in many areas of science and technology.[1−6] In particular, the organization of polymeric or molecular π-conjugated materials into ordered structures in the solid state is important for achieving optimal function of optoelectronic devices, including photovoltaics, field effect transistors, and light emitting diodes.[7−10] In organic semiconductors, the electronic properties are strongly dependent upon the supramolecular structure of the material, which is primarily governed by weak $\pi-\pi$ interactions and van der Waals forces between single molecules or polymer chains. Few guidelines exist for controlling such interactions in a reliable manner as a function of the structure of the molecular components.[11] Even more, bulk properties can be influenced by a number of other factors, including impurities,[12,13] substrate properties,[14] processing conditions,[15−17] and post-deposition treatments.[18−23]

Advantages of organic semiconductors include the possibility for the optoelectronic properties and the solid-state organization to be systematically tuned through molecular design and synthesis[24−26] and/or selective doping.[27] These materials can be processed by thermal evaporation at moderate temperatures or via solution deposition methods, thus allowing for mild processing procedures and the integration of lightweight, flexible substrates into the device architecture.[28−30] Vacuum sublimation is commonly utilized for the fabrication of small-molecule-based devices,[31−37] while solution processing techniques have been largely reserved for polymer-based devices.[38−41] However, recent advances have demonstrated the potential of molecular systems for use in solution-fabricated photovoltaic devices.[21,42−49] Advantages of small molecules over polymers include their well-defined molecular structure−property relationships (i.e., no molecular weight distribution dependence) and the ability to specifically determine the solid-state structure via single-crystal X-ray diffraction(XRD).[50−53]

Received: November 3, 2012
Published: January 8, 2013

Several recent reports have capitalized on the discrete nature of molecular systems to correlate structure to bulk and electronic properties,[34,54−58] but few studies exist that aim to understand the influence of molecular shape on such properties.[59] A study exists that correlated the shape of arylacetylenic-based small molecules to device performance and showed that linear derivatives outperform those that are branched.[60] In a separate study, "zigzag" naphthodithiophene-based small molecules outperformed their linear counterparts.[44,61] More recently, reports have appeared that correlated structural conformation to device performance. There, materials with conformationally "locked" structures led to higher ordered thin films and increased device performance.[62,63]

In this contribution, we first demonstrate how the position of heteroatoms (i.e., pyridyl N-atoms, see Scheme 1) within the π-conjugated backbone of a molecular semiconductor can not only influence the electronic structure but also impact the molecular shape by bending the π-conjugated backbone. These changes at the building block scale translate to different supramolecular assemblies within crystalline domains. Second, we examine the effect of isoelectronic bridgehead substitution within fused dithiophenes (i.e., C vs Si vs Ge) and show how increasing the covalent size of the heteroatom accentuates the bending within the molecular backbone (Scheme 1). Both types of substitution lead to observable differences in bulk self-organization.

Scheme 1. Schematic Summary of Compounds Studied To Determine the Effect of Heteroatom Substitution on Molecular Shape and Supramolecular Arrangement in the Solid State

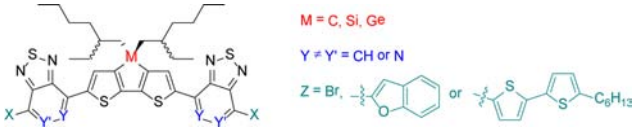

RESULTS AND DISCUSSION

1. Impact of Regiochemistry. *Regiochemical Considerations.* For our initial study we focused on two regioisomers with respect to the pyridyl nitrogens relative to the center of the chromophore, namely 5,5′-bis{7-(4-(benzo[*b*]furan-2-yl))-[1,2,5]thiadiazolo[3,4-*c*]pyridine}-3,3′-di-2-ethylhexylsilylene-2,2′-bithiophene (**1**) and 5,5′-bis{4-(7-(benzo[*b*]furan-2-yl))-[1,2,5]thiadiazolo[3,4-*c*]pyridine}-3,3′-di-2-ethylhexylsilylene-2,2′-bithiophene (**2**) (Figure 1A). Compounds **1** and **2** have a D′ADAD′-type structure, where D/D′ and A correspond to electron-rich and electron-deficient aromatic heterocyclic units, respectively. This type of molecular architecture has proven successful as the basis of designing donor materials for organic solar cell fabrication.[43,47,63,64] The ADA core consists of a central dithienosilole (DTS, donor) unit flanked by two [1,2,5]thiadiazolo[3,4-*c*]pyridine (PT, acceptor) units. 2-Benzofuran (BzFu) units end-cap the molecule to increase π-conjugation and narrow the optical bandgap. Note that compounds **1** and **2** are regioisomers that differ only in the position of the pyridyl N-atoms. The pyridyl N-atoms are located *distal* and *proximal* to the DTS central unit for **1** and **2**, respectively. While chemical intuition would suggest that **1** and **2** should show only marginal differences in material properties, significant differences were observed for both molecular and bulk properties in the solid state, as discussed below.

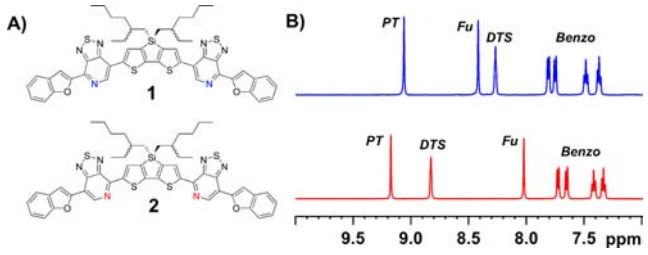

Figure 1. (A) Structures of compounds **1** and **2**. (B) Aromatic region of ^{1}H NMR spectra of compounds **1** (top, blue) and **2** (bottom, red) in $C_2D_2Cl_4$. PT = proton resonance of the [1,2,5]thiadiazolo[3,4-*c*]pyridine fragment, DTS = aromatic proton resonance of the 3,3′-di-2-ethylhexylsilylene-2,2′-bithiophene fragment, Fu = proton resonance in 3-position of 2-benzofuran, Benzo = proton resonances in 4, 5, 6, and 7 positions of 2-benzofuran.

NMR Spectroscopy. Examination by using NMR spectroscopy provides initial evidence that the position of the pyridyl N-atoms affects the distribution of electron density within the molecular backbone. The aromatic regions of the ^{1}H NMR spectra of **1** and **2** are shown in Figure 1B. For both **1** and **2**, the PT proton resonances are farthest shifted downfield, appearing at 9.03 and 9.18 ppm, respectively. Differences between the two spectra are also observed for the DTS and furan resonance peaks. For **1** the furan proton is adjacent to the pyridyl N-atom and, as a result, is downfield shifted 0.45 ppm compared to that in **2**. Likewise for **2**, where the DTS proton is now adjacent to the pyridyl N-atom, a downfield shift of 0.63 ppm is observed relative to that in **1**. The downfield shifts can be attributed to the electron-withdrawing ability of the pyridyl heterocycle, which removes electron density from the respective adjacent regions of the molecule. No significant differences (Supporting Information) are observed in the benzo and aliphatic resonances for **1** and **2**, indicating that the local environments are not perturbed by the position of pyridyl N-atoms. Both compounds exhibit similar temperature-dependent ^{1}H NMR spectra, with both the PT and DTS resonances shifting downfield with increasing temperature. Considering that NMR experiments can be used to gauge aggregation behavior in solution,[65,66] we conclude that, while the position of the pyridyl N-atoms affects the electronic nature of the molecules, there is no major difference in intermolecular solution interactions at these concentrations.

Optical Spectroscopy. Figure 2A provides the optical absorption spectra of **1** and **2** in solution and as spin-cast thin films. Both compounds show similar onsets of absorption

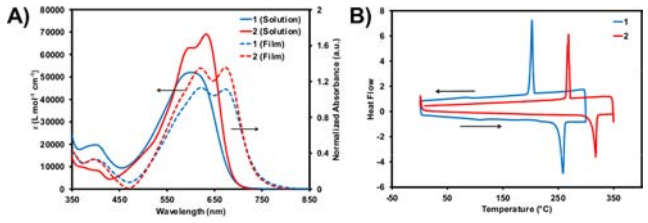

Figure 2. (A) Optical absorption spectra of compounds **1** (blue) and **2** (red) in chlorobenzene solution (solid lines) and as-cast thin films from chlorobenzene on quartz (dashed lines, spectra are normalized to the high energy band). (B) DSC plots for compounds **1** and **2**; scan rate = 10 °C min^{-1}.

dx.doi.org/10.1021/ja310694t | *J. Am. Chem. Soc.* 2013, 135, 2298−2305

in solution (ca. 700 nm) but differ in spectral shape and intensity. The dual-band absorption profile of **1**, with a broad and featureless low-energy band (λ_{max} = 600 nm) and a less intense high-energy band (λ_{max} = 400 nm), is typical of D−A compounds.[67] In contrast, **2** has a higher maximum molar absorptivity (ε = 66 000 vs 54 000 cm^{-1} M^{-1}, Supporting Information Table S6) and shows fine structure within the lowest energy band centered at ∼615 nm ($\lambda_{max1,2}$ = 632 and 598 nm). In conjugated polymer systems, absorption fine structure in solution has been frequently attributed to multichromophore aggregation.[68−70] Changing the temperature or concentration in solution can affect this aggregation and alter the absorption profile.[71−74] However, heating solutions of **2** above 100 °C or decreasing the concentration by a full order of magnitude resulted in no changes to the absorption profile (Supporting Information). This observation implies that the fine structure observed in the solution absorption of **2** is likely intrinsic to the single molecule and may indicate restricted intramolecular motion.[75] Note that the thin-film spectra in Figure 2A were normalized because of differences in thickness. Compared to solution, the film spectra are red-shifted by ∼70 nm and show two distinct peaks within the low-energy band. Such features are attributed to increased π-conjugation length due to planarization of the molecule and intermolecular $\pi-\pi$ interactions.[74,76]

Thermal Properties and Solubility. The position of the pyridyl N-atom has a noticeable impact on the thermal properties of the materials. Thermal transitions of **1** and **2** were investigated using differential scanning calorimetry (DSC), and the resulting traces are shown in Figure 2B. Compared to **1**, the melting and crystallization temperatures for **2** are increased by 59 and 66 °C, respectively. These increases in thermal transition temperatures imply that **2** likely exhibits more and/or stronger intermolecular interactions in the solid state. It is worth noting that the melting temperature of **2** is unusually high for small molecules incorporating bulky alkyl side chains,[57,64] and is similar to that of low side-chain-density materials developed for thermal evaporation.[56] Another consequence of pyridyl N-atom position is solubility in organic solvents. While compound **1** readily dissolves at room temperature in organic solvents such as chloroform and chlorobenzene, **2** does not readily dissolve. For example, the measured solubilities in chlorobenzene for **1** and **2** were determined to be 15 and 2 mg/mL, respectively. The lower solubility of **2** compared to **1** is striking, but is consistent with the higher melting temperature. A practical consequence of the low solubility of **2** that concerns device incorporation is that relatively thick films would only be formed from hot solutions or sequential drop-casting from dilute solutions.

Thin-Film Morphology. Thin-film microstructure was examined by polarized optical microscopy (POM) and XRD. POM images of spin-coated thin films of **1** and **2** are shown in Figure 3. Films were spin-cast from heated 0.5 wt% chlorobenzene solutions at 1000 rpm onto quartz substrates; full experimental details can be found in the Supporting Information. Compound **1** exhibits a homogenously crystalline thin film, while the thin film of **2** consists of regions with large crystallites up to 10 μm in size. Similar observations are observed for drop-cast films, with **2** exhibiting inhomogeneous thin films with domains of large crystallite formation (Supporting Information). The large crystals observed with **2** are consistent with the higher crystallization temperature and lower solubility. Another implication is that, in concentrated solution, **2** might not fully be dissolved and may be present in the form of aggregates.

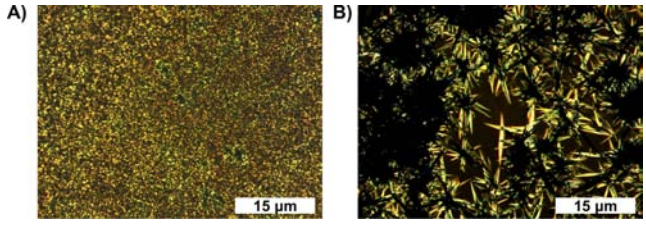

Figure 3. POM images of thin films of (A) **1** and (B) **2**.

Thin-film XRD patterns are shown in Figure 4. Both materials have strong low- and high-angle reflections.

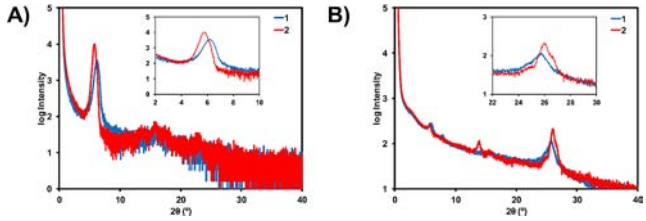

Figure 4. XRD patterns of films of compounds **1** (blue) and **2** (red): (A) out-of-plane and (B) in-plane measurements.

Compounds **1** and **2** exhibit reflections in the out-of-plane measurement at 5.97° and 5.66°, respectively. These values correspond to a *d*-spacing of 14.80 and 15.61 Å, respectively, and are most reasonably associated with the lattice spacing for the alkyl groups. Strong in-plane reflections at 25.70° (3.47 Å) and 26.01° (3.43 Å) are observed for **1** and **2**, respectively, and are associated with the $\pi-\pi$ stacking distance. Smaller diffraction peaks are observed at 7.75° (11.41 Å) for **1** and 13.87° (6.39 Å) for **2**. The similarity in the high angle diffractions implies that intermolecular $\pi-\pi$ distances are similar for both **1** and **2**, but the differences in the other diffraction peaks suggest different crystal packing.

Single-Crystal XRD Studies. For insight into differences in the lattice packing in **1** and **2**, we unambiguously determined their arrangements by single-crystal XRD. Crystals suitable for analysis were grown via slow diffusion of pentane into a carbon disulfide solution (**1**), or diffusion of ether into a carbon disulfide solution (**2**) at 4 °C. Details on structure refinement can be found in the Supporting Information, and the results of these studies for **1** and **2** are summarized in Figures 5 and 6, respectively. It can be seen that both molecules adopt a "banana"-type geometry with the sulfur atoms of the PT and DTS fragments *trans* to one another. Most notably, the degrees of bending within the molecules are different. By measuring the angle between the Si bridgehead atom and the centroids in the PT rings, one determines that compound **1** has a bend angle of 116.1°, while that of compound **2** is 112.0°. Two effects that may contribute to the sharper bending in **2** as compared to **1** include an attractive intramolecular N---S interaction[77] and **1** having a possibly repulsive C−H---S interaction, resulting in increased steric demand. With respect to the former, the N---S distance of 2.89 Å is less than the sum of the corresponding van der Waals radii (∼3.5 Å),[78] and thus the atoms can be described as weakly interacting. Such N---chalcogen interactions are known in the literature and have been described as arising from the donation of the nitrogen lone pair into a low-lying empty *d*-orbital on the chalcogen atom.[79−84]

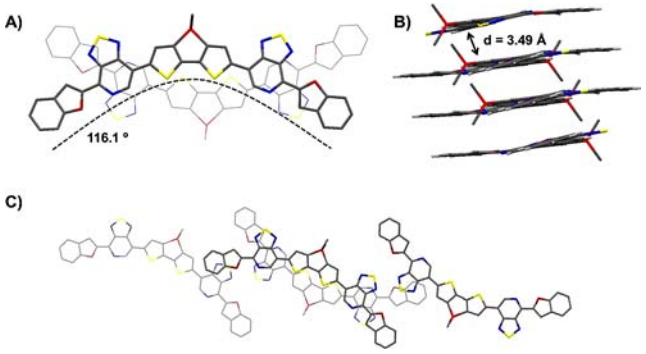

Figure 5. Single-crystal X-ray analysis of **1**: monoclinic, $P2_1/c$. Cell: a = 7.6146(4) Å, b = 33.1008(17) Å, c = 17.9711(9) Å, β = 99.724(3)°, V = 4464.53 Å^3, $R1$ = 0.0586. Atoms: carbon, gray; nitrogen, blue; silicon, red; sulfur, yellow; oxygen, dark red. (A) Face-on view highlighting bend of molecule and intermolecular face-to-face stacking (dashed lines added to highlight molecular bending). (B) Side-on view showing $\pi-\pi$ stacking. (C) Face-on view showing parallel interactions. Alkyl side chains at Si and H atoms are omitted for clarity.

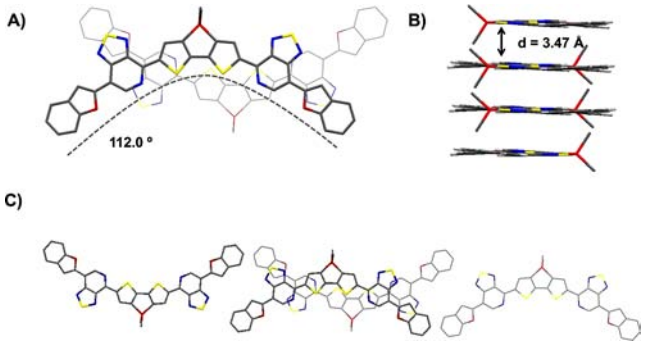

Figure 6. Single-crystal X-ray analysis of **2**: monoclinic, $P\bar{1}$. Cell: a = 8.7918(4) Å, b = 15.5384(7) Å, c = 17.5548(7) Å, α = 74.499(3)°, β = 99.724(3)°, γ = 89.923(3), V = 2299.43 Å^3, $R1$ = 0.0772. Atoms: carbon, gray; nitrogen, blue; silicon, red; sulfur, yellow; oxygen, dark red. (A) Face-on view highlighting bend of molecule and intermolecular face-to-face stacking (dashed lines added to highlight molecular bending). (B) Side-on view showing $\pi-\pi$ stacking. (C) Face-on view showing parallel interactions. Alkyl side chains at Si and H atoms are omitted for clarity.

The geometry (i.e., bend angle of π-conjugated backbone) of the molecules has a significant impact on the crystal organization. While both molecules exhibit short $\pi-\pi$ intermolecular stacking distances of ~3.5 Å, compound **1** packs in a more cofacial arrangement with greater DTS---DTS overlap, while **2** has a greater slip-stack orientation with short contacts between the DTS and PT units (Figures 5C and 6C). Furthermore, **1** has a more compact unit cell (~3% smaller volume per molecule) than **2**. Both compounds organize into assemblies of columnar stacks (Figure 7). In the case of **1**, adjacent stacks are offset, leading to a zigzag orientation, while for **2** aligned stacks are observed. It is reasonable to anticipate that these differences in lattice arrangement lead to the observed differences in thermal properties and argue in favor of changes in charge carrier transport. It is noted that, for polymeric systems, the predicted curvature of the polymer backbone has been shown to influence supramolecular organization and dramatically affect device performance.[85,86]

The powder patterns predicted from the single-crystal structures qualitatively match the thin-film XRD patterns

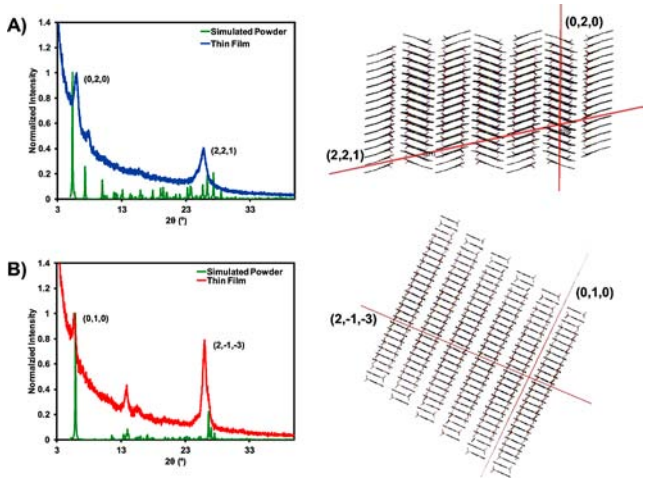

Figure 7. In-plane XRD plots and simulated powder patterns from single-crystal studies for compounds **1** (A) and **2** (B) and a visual description of the primary lattices planes obtained from the single-crystal X-ray structures.

shown in Figure 7. The mismatch between predicted powder patterns and the thin-film patterns is common for organic semiconductors, and it is thought to arise from small changes of cell dimensions (i.e., contractions or enlargements) within thin-film samples and strain within the crystallites.[55−57] Therefore, in the present case it is assumed that similar packing motifs exist in the thin films as in the single crystal, and thus assignments of lattice planes can be made. For **1**, the Bragg reflections at 5.97° and 25.70° are attributed to the (0,2,0) and (2,2,1) planes, while for **2** the Bragg reflections at 5.66° and 26.01° are attributed to the (0,1,0) and (2,−1,−3) planes (Figure 7). For both compounds, the planes giving rise to low-angle reflections run parallel to the $\pi-\pi$ stacks, while the planes giving rise to high-angle reflections run perpendicular to the $\pi-\pi$ stacks and in the direction of the alkyl group ordering. Given the similarities between the calculated powder patterns and the experimental thin-film diffraction studies, it is likely that the molecular shape and inter-chromophore arrangement seen in the single-crystal studies translate to the crystalline domains of the thin films.

DFT Calculations. To probe whether differences in the molecular geometries are intrinsic to the molecule or a consequence of solid-state packing interactions, we investigated the gas-phase structures of **1** and **2** using DFT calculations at the B3LYP/6-31G(d,p) level of theory. As shown in the Supporting Information, the optimized chemical structures are bent in a similar fashion to the experimental solid-state structures, thus implying that there is an intramolecular driving force for adopting the observed molecular configurations. It also appears that the presence of intramolecular N---S interactions aids in the stabilization of the structural conformation. Theoretical calculations revealed that the conformation of **2** shown in Figure 1 is the most stable conformation by 13 kJ/mol, whereas the conformation of **1** shown in Figure 1 is more stable by only 6 kJ/mol (see Supporting Information). Such "conformational locks" have recently been shown to lead to increased supramolecular order in the solid state and subsequent improved electronic performance.[63]

2. Impact of Isoelectronic Bridgehead Substitution. *Bridgehead Atom Effect in the Solid-State Structure.* It

dx.doi.org/10.1021/ja310694t | J. Am. Chem. Soc. 2013, 135, 2298−2305

seemed reasonable that the differences in molecular bend observed for **1** and **2** would not depend solely on the PT regiochemistry, but could also be modulated by the nature of the dithiophene bridging heteroatom. We thus investigated the solid-state structure, as determined by single-crystal diffraction studies, of the PT-D-PT-dibromide precursor of **2** (i.e., compound **3** in Figure 8) and the corresponding isoelectronic

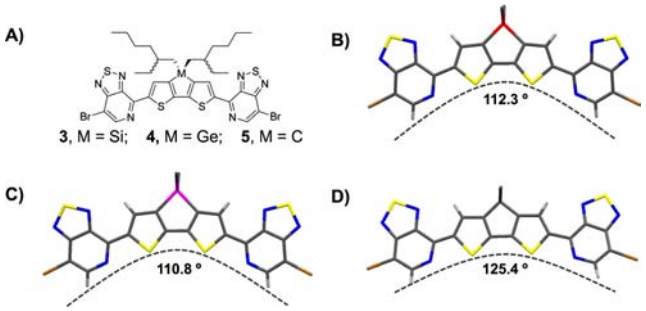

Figure 8. (A) Chemical structures of PT-D-PT-dibromide precursor compounds **3**, **4**, and **5**. Single-crystal analysis of (B) silicon-bridged compound **3**, (C) germanium-bridged compound **4**, and (D) carbon-bridged compound **5**. Atoms: carbon, gray; nitrogen, blue; silicon, red; sulfur, yellow; germanium, purple.

germanium (**4**) and carbon (**5**) analogues. Please refer to Figure 8 for the chemical structures; full synthetic, spectroscopic, and crystallographic data can be found in the Supporting Information. The measured angle between the PT centroids and the Si atom of **3** (Figure 8B) is 112.3°, similar to that of **2** which has the same PT-D-PT core. BzFu-for-Br substitution at the peripheral unit thus does not change the shape of the internal chromophore core. Substituting the Si for Ge atom (**4**, Figure 4C) results in a decrease in the bend angle to 110.8°, due to the larger Ge atom forcing the two thiophene atoms away from one another. A greater increase in bend angle, 125.4° for **5**, is observed upon C-for-Si substitution. In essence, **5** is more linear than **3** and **4**. The average M−C_T bond lengths (where C_T is the thiophenyl carbon atom bound to M) are 1.89, 1.96, and 1.54 Å for **3** (M = Si), **4** (M = Ge), and **5** (M = C), respectively.

Differences in the molecular shape due to heteroatom substitution (i.e., C vs Si vs Ge) are of particular interest with respect to organic π-conjugated materials for photovoltaics. C-, Si-, or Ge-fused dithiophenes have been extensively used as the *donor* component in a variety of high-performance donor−acceptor-type oligomers and polymers.[41,87−89] In most cases it has been found that Si or Ge derivatives lead to improved thin-film order and higher photovoltaic performance when compared to their C analogues.[73,90−92] It has been hypothesized that the longer Si−C_{alkyl}[93] and Ge−C_{alkyl}[94,95] bond lengths reduce side-chain interactions, leading to strong $\pi-\pi$ interactions. In addition to increased M−C_{alkyl} bond lengths, changes in molecular or repeat unit shape, as revealed by comparison of **3**−**5**, are likely to be responsible for the observed differences in thin-film nanostructure and photovoltaic performance.

DFT calculations reveal that the changes in molecular shape are intrinsic to the molecules, with the change in bend angle being reproduced in gas-phase calculations. Going from carbon (**5**) to silicon (**3**) to germanium (**4**) results in decreasing PT(centroid)−bridgehead−PT(centroid) angles of 128.2°, 112.6°, 110.4°, respectively, which correlates well with the measured angles of 125.4°, 112.3°, and 110.8° from the single-crystal data (Figure 8).

Extension of Conjugation. To better understand the effect of molecular structure on shape and bulk properties, we extended the conjugation of compounds **3**, **4**, and **5** by attaching 2-hexylbithiophene end-caps (Figure 9A). Compound

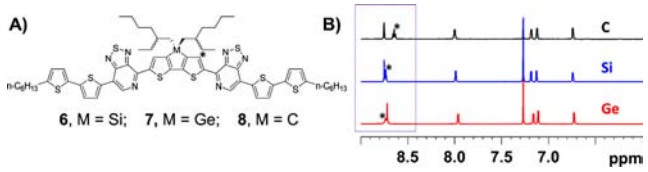

Figure 9. (A) Chemical structures of compounds **6**−**8**. (B) Aromatic region in the ^{1}H NMR spectra of compounds **8** (top, black), **6** (middle, blue), and **7** (bottom, red) in $CDCl_3$. PT and DTS aromatic proton resonances are highlighted with the dashed box.

6 has previously been reported and exhibited excellent power conversion efficiency of 7% when paired with $PC_{71}BM$ in solution-processed bulk heterojunction solar cells.[47,63] While we were not able to obtain X-ray-quality single crystals of **7** or **8**, single-crystal XRD of **6** exhibits the same bend angle between the Si atom and the centroids of the PT units as seen for **3**.[96] On this basis, we assume that the trends observed for **3**−**5** hold similarly for **6**−**8**.

The aromatic region of the ^{1}H NMR spectra for **6**−**8** is shown in Figure 9B. The compounds exhibit similar spectra except for the resonance attributed to the proton in the 4-position of the bridged dithiophene (denoted with an asterisk). A slight downfield shift is observed upon changing from Si to Ge, with the shift between **6** and **7** (ca. 0.05 ppm) less than the shift between **8** and **6** (ca. 0.09 ppm). This shift in resonance indicates a change in the electron density and ring currents within the central core of the molecule due to modulation of the bridgehead atom (full spectra for **6**−**8** can be found in the Supporting Information).

Compounds **6**−**8** exhibit similar electrochemical properties, as determined by cyclic voltammetry (CV), with the carbon compound (**8**) having slightly higher HOMO and LUMO energy levels (Supporting Information, Table S7). Solution optical absorption spectra are shown in Figure 10A. All three

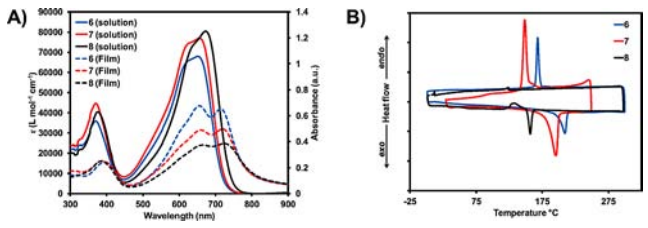

Figure 10. (A) Optical absorption spectra of compounds **6** (blue), **7** (red), and **8** (black) in chlorobenzene solution (solid lines) and as-cast thin films (~120 nm thickness, not normalized) from chlorobenzene on quartz (dashed lines). (B) DSC plots for compounds **6**−**8**. Scan rate = 10 °C min^{-1}.

compounds exhibit similar absorption profiles, with **8** being slightly red-shifted and having a more intense absorption. Thin films of **6**−**8** exhibit broad optical absorption extending beyond 800 nm with different optical densities (Figure 10A). The Si and Ge compounds **6** and **7** show an increase in intensity and fine structure for the low-energy band when compared to the

dx.doi.org/10.1021/ja310694t | J. Am. Chem. Soc. 2013, 135, 2298−2305

carbon compound (**8**), with **6** having the most pronounced low-energy feature. We currently do not have an explanation for the difference in absorption intensity observed for the series when going for solution to solid state.

The thermal properties of **6**–**8** were evaluated using DSC, and the traces are shown in Figure 10B. Both **6** and **7** display distinct melting transitions (209 and 196 °C, respectively) on heating and crystallization transitions (168 and 150 °C, respectively) on cooling. Compound **8** shows a melting transition at 157 °C, a cold crystallization transition at ∼132 °C, and no discernible crystallization on cooling. These results imply that the Si compound **6** has the most stable and possibly ordered bulk structure, consistent with the absorption spectra. It is also worth noting that the distal regioisomer of compound **6** exhibits melting (210 °C) and crystallization (169 °C) temperatures similar to those of **6** (207 and 168 °C, respectively).[63,64]

Further insight into the crystalline nature of the thin films was sought by using XRD (Figure 11). The XRD patterns

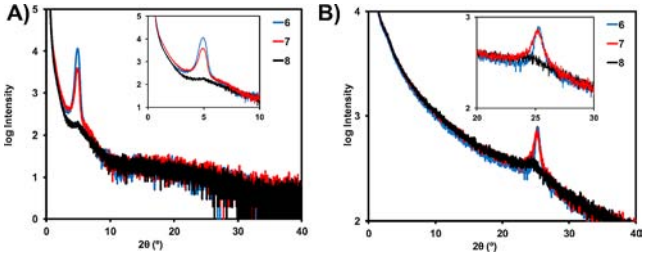

Figure 11. XRD patterns of films of compounds **6** (blue), **7** (red), and **8** (black): (A) out-of-plane and (B) in-plane measurements.

indicate higher crystallinity for **6** and **7** compared to **8**, with more defined diffraction signals at $2\theta \approx 5.0°$ (Figure 11A) and $2\theta \approx 25°$ (Figure 11B) for both **6** and **7**. The similarity in diffraction patterns suggests similar thin-film structures for **6** and **7**.

From the accumulated set of characterization tools utilized, we can ascertain that the Si- (**6**) and Ge-based (**7**) materials have similar molecular and bulk properties and show a strong tendency to form ordered structures in the solid state. In contrast, the C-based material (**8**) does not appear to achieve a similar degree of organization. Correlating these observations to the observed bending seen for **3**–**5**, we conclude that, at least within this set of materials, the greater bend within the Si and Ge molecules results in a stronger tendency to provide crystalline domains under these conditions.

■ CONCLUSION

A series of molecules described by the general D′ADAD′ structure, where D/D′ are electron-rich and A are electron-poor heterocycles, was designed and examined to probe how changes in chemical structure lead to differences in molecular shape and, ultimately, solid-state arrangements. The specific class of molecules relates to materials that serve as the donor component in high-efficiency solution-deposited bulk heterojunction molecular solar cells and is relevant for understanding more generally the organization of organic semiconductors.

Compounds **1** and **2** contain the 3,3′-di-2-ethylhexylsilylene-2,2′-bithiophene fragment as D and benzofuran as D′; they differ insofar that the regiochemistry of the two [1,2,5]-thiadiazolo[3,4-*c*]pyridine heterocycles, corresponding to the A component, can be either *distal* (**1**) or *proximal* (**2**), relative to the interior of the chromophore. Although these structural differences are subtle (see their molecular depictions in Figure 1A) and there is little difference in their absorption profiles (Figure 2A), one finds that the two materials have very different thermal transitions. The melting temperature of compound **2** (317 °C) is approximately 59 °C larger than that of **1** (258 °C). Related to this relatively more stable crystalline lattice, one finds that **2** is much less soluble than **1** in common organic solvents and that the crystallite sizes are much greater in spin-cast films. Such differences in solubility and bulk morphology are of practical relevance when considering options for deposition of semiconducting thin films and are difficult to predict *a priori* exclusively on the basis of chemical structure considerations. Insights into the differences in molecular shape and lattice arrangements were found via single-crystal XRD studies. We find it particularly noteworthy that, while both **1** and **2** generally exhibit the same banana-like conformation, the bend angle for **2** is considerably smaller (112.0° vs 116.1°). This difference is attributed to the ability of the pyridyl nitrogens to interact with the sulfur atoms within the linked bithiophene unit, which provides a driving force for molecular deformation (see Scheme 2). Intramolecular N---S coordination of this type has been previously observed in several other molecular systems and has been used to understand, for example, the preferential geometries of sulfur-containing diazenes.[80,83] We also find that **1** and **2** pack in different arrangements within the crystalline lattice. The degree to which the molecular topology influences these preferences for organization has not been determined at this stage, and likely there are additional contributing factors, such as the differences in the orientation of the terminal BzFu fragments. It is also relevant that, for proximal and distal isomers of **6**, one finds nearly identical melting and crystallization temperatures. As such, the effect of bending on bulk properties can be "washed out" by longer end-capping groups and other competing forces. Regardless of these uncertainties, it is interesting to note that the simulated powder fragments from the single-crystal determinations match those obtained from thin films. What is learned from crystallographic analysis is therefore relevant for understanding the structure and local environment in the active layers of organic optoelectronic devices.

Scheme 2. Intramolecular N---S Interactions Accentuate Bending of the Molecular Framework

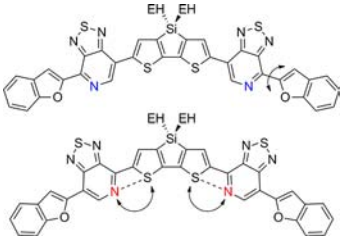

The series of compounds **3** (Si), **4** (Ge), and **5** (C) can be used to examine the effect of different bridgehead atoms in the internal fused dithiophene substructure. As the length of the M–C_T bond increases proportionally to the covalent radii of M (111 pm, **3**; 120 pm, **4**; 76 pm, **5**), there is a commensurate molecular bend (112.3°, **3**; 110.8°, **4**; 125.4°, **5**) (see Scheme 3). These effects likely work in tandem with the N---S coordination mentioned above. Compound **6**, which has been

dx.doi.org/10.1021/ja310694t | *J. Am. Chem. Soc.* 2013, 135, 2298–2305

Scheme 3. Increasing the M−C_T Bond Length Accentuates Bending of the Molecular Framework

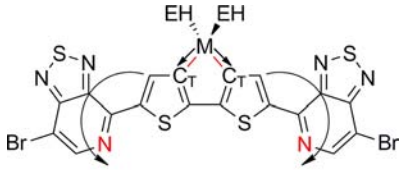

M = Si (**3**), Ge (**4**), C (**5**)

successfully integrated within organic photovoltaic devices, and which differs from **3** insofar as the end group of the molecule is 5-hexylbithiophene instead of bromide, exhibits the same bend angle. It is therefore likely that the structural details of **4** and **5** extend to **7** and **8**, respectively. Furthermore, as seen in the case of **1** and **2**, there is a qualitative correlation between the increased bending in **6** and **7**, versus **8**, and increasing melting temperature and propensity to form crystallites.

These model studies highlight a potential advantage of solution-deposited molecular organic semiconductor materials, relative to polymeric counterparts: they offer the possibility of facile fabrication methods while at the same time providing insight into the precise arrangement of molecular subunits in the solid state.

■ ASSOCIATED CONTENT

Ⓢ Supporting Information

Materials and methods; synthetic and spectroscopic details of **2**−**5**, **7**, and **8**; temperature and concentration-dependent UV−vis spectroscopy of **2**; temperature-dependent ^{1}H NMR spectra of **1** and **2**; CV of **2**; POM images of **1** and **2**; powder XRD; and theoretical calculations. This material is available free of charge via the Internet at http://pubs.acs.org.

■ AUTHOR INFORMATION

Corresponding Author

bazan@chem.ucsb.edu

Present Address

[§]Department of Chemistry, Dalhousie University, Halifax, Nova Scotia, Canada

Notes

The authors declare no competing financial interest.

■ ACKNOWLEDGMENTS

Support was provided by the Center for Energy Efficient Materials, an Energy Frontier Research Center funded by the Office of Basic Energy Sciences of the U.S. Department of Energy (DE-DC0001009). We acknowledge support from the Center for Scientific Computing at the CNSI and MRL: an NSF MRSEC (DMR-1121053) and NSF CNS-0960316. Neil Treat (UCSB) is acknowledged for assistance with optical microscopy imaging. The Advanced Light Source is supported by the Director, Office of Science, Office of Basic Energy Sciences of the U.S. Department of Energy under Contract No. DE-AC02-05CH11231.

■ REFERENCES

(1) Whitesides, G.; Mathias, J.; Seto, C. *Science* **1991**, *254*, 1312.
(2) Whitesides, G.; Grzybowski, B. *Science* **2002**, *295*, 2418.
(3) Ikkala, O.; ten Brinke, G. *Science* **2002**, *295*, 2407.
(4) Lehn, J. *Science* **2002**, *295*, 2400.
(5) Reinhoudt, D.; Crego-Calama, M. *Science* **2002**, *295*, 2403.
(6) Palma, C.; Cecchini, M.; Samori, P. *Chem. Soc. Rev.* **2012**, *41*, 3713.
(7) Hoeben, F.; Jonkheijm, P.; Meijer, E.; Schenning, A. *Chem. Rev.* **2005**, *105*, 1491.
(8) Beaujuge, P.; Frechet, J. *J. Am. Chem. Soc.* **2011**, *133*, 20009.
(9) Mas-Torrent, M.; Rovira, C. *Chem. Rev.* **2011**, *111*, 4833.
(10) Zhou, H.; Yang, L.; You, W. *Macromolecules* **2012**, *45*, 607.
(11) Henson, Z. B.; Müllen, K.; Bazan, G. C. *Nature Chem.* **2012**, *4*, 699.
(12) Cowan, S.; Leong, W.; Banerji, N.; Dennler, G.; Heeger, A. *Adv. Funct. Mater.* **2011**, *21*, 3083.
(13) Leong, W. L.; Welch, G. C.; Kaake, L. G.; Takacs, C. J.; Sun, Y.; Bazan, G. C.; Heeger, A. J. *Chem. Sci.* **2012**, *3*, 2103.
(14) Garcia, A.; Welch, G. C.; Ratcliff, E. L.; Ginley, D. S.; Bazan, G. C.; Olson, D. C. *Adv. Mater.* **2012**, *24*, 5368.
(15) Wienk, M.; Turbiez, M.; Gilot, J.; Janssen, R. *Adv. Mater.* **2008**, *20*, 2556.
(16) Peet, J.; Senatore, M. L.; Heeger, A. J.; Bazan, G. C. *Adv. Mater.* **2009**, *21*, 1521.
(17) Kronenberg, N.; Steinmann, V.; Burckstummer, H.; Hwang, J.; Hertel, D.; Wurthner, F.; Meerholz, K. *Adv. Mater.* **2010**, *22*, 4193.
(18) Gregg, B. *J. Phys. Chem.* **1996**, *100*, 852.
(19) Conboy, J.; Olson, E.; Adams, D.; Kerimo, J.; Zaban, A.; Gregg, B.; Barbara, P. *J. Phys. Chem. B* **1998**, *102*, 4516.
(20) Verploegen, E.; Mondal, R.; Bettinger, C.; Sok, S.; Toney, M.; Bao, Z. *Adv. Funct. Mater.* **2010**, *20*, 3519.
(21) Wei, G.; Wang, S.; Sun, K.; Thompson, M.; Forrest, S. *Adv. Energy Mater.* **2011**, *1*, 184.
(22) Zimmerman, J.; Xiao, X.; Renshaw, C.; Wang, S.; Diev, V.; Thompson, M.; Forrest, S. *Nano Lett.* **2012**, *12*, 4366.
(23) Park, Y.; Park, J.; Lee, W.; Kang, B.; Cho, K.; Bazan, G. *J. Mater. Chem.* **2012**, *22*, 11462.
(24) Cheng, Y.; Yang, S.; Hsu, C. *Chem. Rev.* **2009**, *109*, 5868.
(25) Jung, B.; Tremblay, N.; Yeh, M.; Katz, H. *Chem. Mater.* **2011**, *23*, 568.
(26) Gibson, G. L.; McCormick, T. M.; Seferos, D. S. *J. Am. Chem. Soc.* **2012**, *134*, 539.
(27) Welch, G. C.; Bazan, G. C. *J. Am. Chem. Soc.* **2011**, *133*, 4632.
(28) Forrest, S. R. *Nature* **2004**, *428*, 911.
(29) Sondergaard, R.; Hosel, M.; Angmo, D.; Larsen-Olsen, T.; Krebs, F. *Mater. Today* **2012**, *15*, 36.
(30) Kaltenbrunner, M.; White, M.; Glowacki, E.; Sekitani, T.; Someya, T.; Sariciftci, N.; Bauer, S. *Nat. Commun.* **2012**, *3*, 770.
(31) Peumans, P.; Uchida, S.; Forrest, S. R. *Nature* **2003**, *425*, 158.
(32) Riede, M.; Mueller, T.; Tress, W.; Schueppel, R.; Leo, K. *Nanotechnology* **2008**, *19*, 424001.
(33) Hains, A.; Liang, Z.; Woodhouse, M.; Gregg, B. *Chem. Rev.* **2010**, *110*, 6689.
(34) Lin, L.; Chen, Y.; Huang, Z.; Lin, H.; Chou, S.; Lin, F.; Chen, C.; Liu, Y.; Wong, K. *J. Am. Chem. Soc.* **2011**, *133*, 15822.
(35) Steinmann, V.; Kronenberg, N.; Lenze, M.; Graf, S.; Hertel, D.; Meerholz, K.; Burckstummer, H.; Tulyakova, E.; Wurthner, F. *Adv. Energy Mater.* **2011**, *1*, 888.
(36) Chen, Y.-H.; Lin, L.-Y.; Lu, C.-W.; Lin, F.; Huang, Z.-Y.; Lin, H.-W.; Wang, P.-H.; Liu, Y.-H.; Wong, K.-T.; Wen, J.; Miller, D. J.; Darling, S. B. *J. Am. Chem. Soc.* **2012**, *134*, 13616.
(37) Chiu, S.; Lin, L.; Lin, H.; Chen, Y.; Huang, Z.; Lin, Y.; Lin, F.; Liu, Y.; Wong, K. *Chem. Commun.* **2012**, *48*, 1857.
(38) Pron, A.; Rannou, P. *Prog. Polym. Sci.* **2002**, *27*, 135.
(39) Gunes, S.; Neugebauer, H.; Sariciftci, N. S. *Chem. Rev.* **2007**, *107*, 1324.
(40) Krebs, F. *Sol. Energy Mater. Sol. Cells* **2009**, *93*, 394.
(41) Li, G.; Zhu, R.; Yang, Y. *Nat. Photonics* **2012**, *6*, 153.
(42) Walker, B.; Tomayo, A.; Dang, X.; Zalar, P.; Seo, J.; Garcia, A.; Tantiwiwat, M.; Nguyen, T. *Adv. Funct. Mater.* **2009**, *19*, 3063.
(43) Welch, G.; Perez, L.; Hoven, C.; Zhang, Y.; Dang, X.; Sharenko, A.; Toney, M.; Kramer, E.; Nguyen, T.; Bazan, G. *J. Mater. Chem.* **2011**, *21*, 12700.

(44) Loser, S.; Bruns, C.; Miyauchi, H.; Ortiz, R.; Facchetti, A.; Stupp, S.; Marks, T. *J. Am. Chem. Soc.* **2011**, *133*, 8142.
(45) Lee, O. P.; Yiu, A. T.; Beaujuge, P. M.; Woo, C. H.; Holcombe, T. W.; Millstone, J. E.; Douglas, J. D.; Chen, M. S.; Frechet, J. M. J. *Adv. Mater.* **2011**, *23*, 5359.
(46) Burckstummer, H.; Tulyakova, E. V.; Deppisch, M.; Lenze, M. R.; Kronenberg, N. M.; Gsanger, M.; Stolte, M.; Meerholz, K.; Wurthner, F. *Angew. Chem., Int. Ed.* **2011**, *50*, 11628.
(47) Sun, Y.; Welch, G.; Leong, W.; Takacs, C.; Bazan, G.; Heeger, A. *Nat. Mater.* **2012**, *11*, 44.
(48) Li, Z.; He, G. R.; Wan, X. J.; Liu, Y. S.; Zhou, J. Y.; Long, G. K.; Zuo, Y.; Zhang, M. T.; Chen, Y. S. *Adv. Energy Mater.* **2012**, *2*, 74.
(49) Zhou, J.; Wan, X.; Liu, Y.; Zuo, Y.; Li, Z.; He, G.; Long, G.; Ni, W.; Li, C.; Su, X.; Chen, Y. *J. Am. Chem. Soc.* **2012**, *134*, 16345.
(50) Wurthner, F.; Meerholz, K. *Chem.—Eur. J.* **2010**, *16*, 9366.
(51) Mishra, A.; Bauerle, P. *Angew. Chem., Int. Ed.* **2012**, *51*, 2020.
(52) Wu, C. *MRS Bull.* **2012**, *37*, 2.
(53) Lin, Y.; Li, Y.; Zhan, X. *Chem. Soc. Rev.* **2012**, *41*, 4245.
(54) Fitzner, R.; Reinold, E.; Mishra, A.; Mena-Osteritz, E.; Ziehlke, H.; Korner, C.; Leo, K.; Riede, M.; Weil, M.; Tsaryova, O.; Weiss, A.; Uhrich, C.; Pfeiffer, M.; Bauerle, P. *Adv. Funct. Mater.* **2011**, *21*, 897.
(55) Fitzner, R.; Mena-Osteritz, E.; Mishra, A.; Schulz, G.; Reinold, E.; Weil, M.; Korner, C.; Ziehlke, H.; Elschner, C.; Leo, K.; Riede, M.; Pfeiffer, M.; Uhrich, C.; Bauerle, P. *J. Am. Chem. Soc.* **2012**, *134*, 11064.
(56) Fitzner, R.; Elschner, C.; Weil, M.; Uhrich, C.; Korner, C.; Riede, M.; Leo, K.; Pfeiffer, M.; Reinold, E.; Mena-Osteritz, E.; Bauerle, P. *Adv. Mater.* **2012**, *24*, 675.
(57) Kim, C.; Liu, J. H.; Lin, J. S.; Tamayo, A. B.; Walker, B.; Wu, G.; Nguyen, T. Q. *Chem. Mater.* **2012**, *24*, 1699.
(58) Viterisi, A.; Gispert-Guirado, F.; Ryan, J. W.; Palomares, E. *J. Mater. Chem.* **2012**, *22*, 15175.
(59) Cademartiri, L.; Bishop, K.; Snyder, P.; Ozin, G. *Philos. Trans. R. Soc. A—Math., Phys, Eng. Sci.* **2012**, *370*, 2824.
(60) Seri, M.; Marrocchi, A.; Bagnis, D.; Ponce, R.; Taticchi, A.; Marks, T. J.; Facchetti, A. *Adv. Mater.* **2011**, *23*, 3827.
(61) Loser, S.; Miyauchi, H.; Hennek, J.; Smith, J.; Huang, C.; Facchetti, A.; Marks, T. *Chem. Commun.* **2012**, *48*, 8511.
(62) Huang, H.; Chen, Z.; Ortiz, R. P.; Newman, C.; Usta, H.; Lou, S.; Youn, J.; Noh, Y.-Y.; Baeg, K.-J.; Chen, L. X.; Facchetti, A.; Marks, T. *J. Am. Chem. Soc.* **2012**, *134*, 10966.
(63) Takacs, C. J.; Sun, Y.; Welch, G. C.; Perez, L. A.; Liu, X.; Wen, W.; Bazan, G. C.; Heeger, A. J. *J. Am. Chem. Soc.* **2012**, *134*, 16597.
(64) Henson, Z.; Welch, G.; van der Poll, T.; Bazan, G. *J. Am. Chem. Soc.* **2012**, *134*, 3766.
(65) Wong, W.; Ma, C.; Pisula, W.; Yan, C.; Feng, X.; Jones, D.; Mullen, K.; Janssen, R.; Bauerle, P.; Holmes, A. *Chem. Mater.* **2010**, *22*, 457.
(66) Mayerhöffer, U. W. *Angew. Chem., Int. Ed.* **2012**, *51*, 5615.
(67) Beaujuge, P.; Amb, C.; Reynolds, J. *Acc. Chem. Res.* **2010**, *43*, 1396.
(68) Traiphol, R.; Charoenthai, N.; Srikhirin, T.; Kerdeharoen, T.; Osotchan, T.; Maturos, T. *Polymer* **2007**, *48*, 813.
(69) Scharsich, C.; Lohwasser, R.; Sommer, M.; Asawapirom, U.; Scherf, U.; Thelakkat, M.; Neher, D.; Kohler, A. *J. Polym. Sci., Part B: Polym. Phys.* **2012**, *50*, 442.
(70) Steyrleuthner, R.; Schubert, M.; Howard, I. A.; Klaumünzer, B.; Schilling, K.; Chen, Z.; Saalfrank, P.; Laquai, F.; Facchetti, A.; Neher, D. *J. Am. Chem. Soc.* **2012**, *134*, 18303.
(71) Karsten, B.; Viani, L.; Gierschner, J.; Cornil, J.; Janssen, R. *J. Phys. Chem. A* **2008**, *112*, 10764.
(72) Zoombelt, A. P.; Fonrodona, M.; Turbiez, M. G. R.; Wienk, M. M.; Janssen, R. A. J. *J. Mater. Chem.* **2009**, *19*, 5336.
(73) Coffin, R. C.; Peet, J.; Rogers, J.; Bazan, G. C. *Nature Chem.* **2009**, *1*, 657.
(74) Steyrleuthner, R.; Schubert, M.; Howard, I. A.; Klaumünzer, B.; Schilling, K.; Chen, Z.; Saalfrank, P.; Laquai, F.; Facchetti, A.; Neher, D. *J. Am. Chem. Soc.* **2012**, *134*, 18303.
(75) Karsten, B.; Janssen, R. *Org. Lett.* **2008**, *10*, 3513.
(76) Peet, J.; Cho, N.; Lee, S.; Bazan, G. *Macromolecules* **2008**, *41*, 8655.
(77) Mugesh, G.; Singh, H. B.; Butcher, R. J. *J. Chem. Res.-S* **1999**, 472.
(78) Bondi, A. *J. Phys. Chem.* **1964**, *68*, 441.
(79) Karikomi, M.; Kitamura, C.; Tanaka, S.; Yamashita, Y. *J. Am. Chem. Soc.* **1995**, *117*, 6791.
(80) Chivers, T.; Krouse, I.; Parvez, M.; VargasBaca, I.; Ziegler, T.; Zoricak, P. *Inorg. Chem.* **1996**, *35*, 5836.
(81) Cozzolino, A. F.; Vargas-Baca, I.; Mansour, S.; Mahmoudkhani, A. H. *J. Am. Chem. Soc.* **2005**, *127*, 3184.
(82) Yasuda, T.; Sakai, Y.; Aramaki, S.; Yamamoto, T. *Chem. Mater.* **2005**, *17*, 6060.
(83) Chivers, T. *A Guide To Chalcogen-Nitrogen Chemistry*; World Scientific Publishing Co. Pte. Ltd.: Singapore, 2005.
(84) Mukherjee, A. J.; Zade, S. S.; Singh, H. B.; Sunoj, R. B. *Chem. Rev.* **2010**, *110*, 4357.
(85) Rieger, R.; Beckmann, D.; Mavrinskiy, A.; Kastler, M.; Mullen, K. *Chem. Mater.* **2010**, *22*, 5314.
(86) Guo, X.; Puniredd, S.; Baumgarten, M.; Pisula, W.; Mullen, K. *J. Am. Chem. Soc.* **2012**, *134*, 8404.
(87) Gendron, D.; Leclerc, M. *Energy Environ. Sci.* **2011**, *4*, 1225.
(88) Duan, C. H.; Huang, F.; Cao, Y. *J. Mater. Chem.* **2012**, *22*, 10416.
(89) Small, C.; Chen, S.; Subbiah, J.; Amb, C.; Tsang, S.; Lai, T.; Reynolds, J.; So, F. *Nat. Photonics* **2012**, *6*, 115.
(90) Scharber, M. C.; Koppe, M.; Gao, J.; Cordella, F.; Loi, M. A.; Denk, P.; Morana, M.; Egelhaaf, H. J.; Forberich, K.; Dennler, G.; Gaudiana, R.; Waller, D.; Zhu, Z. G.; Shi, X. B.; Brabec, C. J. *Adv. Mater.* **2010**, *22*, 367.
(91) Morana, M.; Azimi, H.; Dennler, G.; Egelhaaf, H. J.; Scharber, M.; Forberich, K.; Hauch, J.; Gaudiana, R.; Waller, D.; Zhu, Z. H.; Hingerl, K.; van Bavel, S. S.; Loos, J.; Brabec, C. J. *Adv. Funct. Mater.* **2010**, *20*, 1180.
(92) Gendron, D.; Morin, P. O.; Berrouard, P.; Allard, N.; Aich, B. R.; Garon, C. N.; Tao, Y.; Leclerc, M. *Macromolecules* **2011**, *44*, 7188.
(93) Chen, H. Y.; Hou, J. H.; Hayden, A. E.; Yang, H.; Houk, K. N.; Yang, Y. *Adv. Mater.* **2010**, *22*, 371.
(94) Amb, C. M.; Chen, S.; Graham, K. R.; Subbiah, J.; Small, C. E.; So, F.; Reynolds, J. R. *J. Am. Chem. Soc.* **2011**, *133*, 10062.
(95) Kim, J. S.; Fei, Z. P.; James, D. T.; Heeney, M.; Kim, J. S. *J. Mater. Chem.* **2012**, *22*, 9975.
(96) Zhugayevych, A.; Postupna, O.; Bakus, R.; Welch, G.; Bazan, G.; Tretiak, S. **2012**, submitted.